

# Nanoscale

Accepted Manuscript



This is an *Accepted Manuscript*, which has been through the Royal Society of Chemistry peer review process and has been accepted for publication.

*Accepted Manuscripts* are published online shortly after acceptance, before technical editing, formatting and proof reading. Using this free service, authors can make their results available to the community, in citable form, before we publish the edited article. We will replace this *Accepted Manuscript* with the edited and formatted *Advance Article* as soon as it is available.

You can find more information about *Accepted Manuscripts* in the [Information for Authors](#).

Please note that technical editing may introduce minor changes to the text and/or graphics, which may alter content. The journal's standard [Terms & Conditions](#) and the [Ethical guidelines](#) still apply. In no event shall the Royal Society of Chemistry be held responsible for any errors or omissions in this *Accepted Manuscript* or any consequences arising from the use of any information it contains.

## **Ion Transport and Selectivity in Biomimetic Nanopores with pH-Tunable Zwitterionic Polyelectrolyte Brushes**

Zhenping Zeng,<sup>1,+</sup> Li-Hsien Yeh,<sup>2,+,\*</sup> Mingkan Zhang,<sup>3</sup> and Shizhi Qian<sup>4,\*</sup>

<sup>1</sup>School of Electronic and Optical Engineering, Nanjing University of Science and Technology, Nanjing 210094, P. R. China

<sup>2</sup>Department of Chemical and Materials Engineering, National Yunlin University of Science and Technology, Yunlin 64002, Taiwan

<sup>3</sup>Department of Geology and Geophysics, University of Wyoming, Laramie, WY 82071, USA

<sup>4</sup>Institute of Micro/Nanotechnology, Old Dominion University, Norfolk, VA 23529, USA

---

+ These two authors contributed equally to this work

\* Corresponding authors:

Fax: +886-5-5312071; E-mail: [lhyeh@yuntech.edu.tw](mailto:lhyeh@yuntech.edu.tw) (Li-Hsien Yeh),  
[sqian@odu.edu](mailto:sqian@odu.edu) (Shizhi Qian)

**Abstract**

Inspired by nature, functionalized nanopores with biomimetic structures have attracted growing interests in using them as novel platforms for applications of regulating ion and nanoparticle transport. To improve these emerging applications, we study theoretically for the first time the ion transport and selectivity in short nanopores functionalized with pH tunable, zwitterionic polyelectrolyte (PE) brushes. In addition to background salt ions, the study takes into account the presence of  $H^+$  and  $OH^-$  ions along with the chemistry reactions between functional groups on PE chains and protons. Due to ion concentration polarization, the charge density of PE layers is not homogeneously distributed and depends significantly on the background salt concentration, pH, grafting density of PE chains, and applied voltage bias, thereby resulting in many interesting and unexpected ion transport phenomena in the nanopore. For example, the ion selectivity of the biomimetic nanopore can be regulated from anion-selective (cation-selective) to cation-selective (anion-selective) by diminishing (raising) the solution pH when a sufficiently small grafting density of PE chains, large voltage bias, and low background salt concentration are applied.

**Keywords:** Nanofluidics; Nanopore Conductance; Charge Regulation; Ion Concentration Polarization; Chemically Modified Nanopores

## 1. Introduction

Inspired by biological protein channels, synthetic nanopores decorated with a variety of functionalized macromolecules have developed many environmental stimuli, such as pH,<sup>1-9</sup> voltage,<sup>3</sup> temperature,<sup>10</sup> ionic species,<sup>11</sup> and light.<sup>12</sup> Among them, pH-tunable biomimetic nanopores, nanosized pores in solid-state membranes modified with pH-regulated polyelectrolyte (PE) brushes, have attracted more attention due to their potential applications in diverse fields, including energy transduction,<sup>1</sup> ionic gates,<sup>2-5</sup> ionic pumps,<sup>6</sup> nanofluidic diodes<sup>7,8</sup> and biosensors,<sup>9</sup> to name a few. It has been discovered that the performance of these applications is affected significantly by the charge property of PE layers and ionic conductance behavior in the nanopore, which are very sensitive to pH stimuli. Recent studies strongly suggest that as the size of pores is narrowed to the thickness of electric double layer (EDL), unique ion transport properties, not observed in microscale pores, emerge, such as ion selectivity,<sup>13,14</sup> ion concentration polarization (ICP),<sup>15-17</sup> and ion concentration rectification (ICR).<sup>18-20</sup> Considering the growing applications using pH-tunable bioinspired nanopores, a comprehensive understanding of the interplay among the charge property of PE brush layers, conductance, and ion transport behaviors is highly necessary.

Existing theoretical studies focused mainly on the solid-state nanopores.<sup>13, 14, 21-27</sup> Compared with those, available studies on the ion transport in PE layer-modified nanopores are very limited because of the complexity of mathematical model. For instance, Tagliazucchi

et al.<sup>28</sup> investigated the ionic conductance in PE-modified nanopores with considering the molecular organization under an applied electric field. They found that the molecular structure of PE chains deform significantly, which in turn affects the ionic conductance in the nanopore, when the molecular length of PE chains is too long and the applied electric field is large. Applying the same molecular theory, the same group further discussed the possibility of using nanopores with outer membranes functionalized with PE brushes of bipolar charges and found excellent rectification behavior in the nanopore.<sup>29</sup> Until recently, the analyses on the electrokinetic ion<sup>30</sup> and nanoparticle<sup>31, 32</sup> transport, ICP,<sup>33</sup> and ICR<sup>34</sup> in nanopores functionalized with PE brush layers have been made by using the coupled Poisson-Nernst-Planck (PNP) and modified Stokes-Brinkman equations. Nevertheless, the systems described above assumed that the PE brushes carry homogeneously fixed charges, implying that the charge density of PE layers is independent of the solution pH and salt concentration, and only considered the influence of the background salt ions on the conductance behavior in the nanopore. The understanding of the pH-tunable biomimetic nanopores is therefore still very limited by the fact that the presence of  $H^+$  and  $OH^-$  ions is often neglected, and its response to and its impact on the charge density of PE brush layers and other ion transport phenomena (e.g., ion selectivity and ICP) have not been investigated.

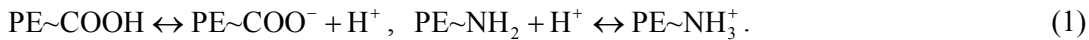
In this work, we present the first theoretical attempt to investigate the ionic conductance, ICP, and ion selectivity in a pH tunable, zwitterionic PE brush-functionalized nanopore as

functions of the background salt concentration, pH, grafting density of PE chains, and applied voltage bias. To mimic the pH-tunable nature of bioinspired nanopores, our model extends the previous continuum-based model (see Theoretical Model section), which has been verified and is suitable for describing the underlying physics of ion transport in PE layer-modified nanopores,<sup>30-33</sup> to the more general case with considering the presence of  $H^+$  and  $OH^-$  ions and chemistry reactions of the functional groups on PE chains. We show that the ion selectivity of the nanopore can be actively regulated by adjusting the solution pH under certain conditions.

## 2. Theoretical Model

As schematically shown in Fig. 1, we considered a cylindrical nanopore of radius  $R_n$  and length  $L_n$  fabricated in a solid-state membrane, which separates two large, identical reservoirs of radius  $R_r$  and length  $L_r$ . Both the nanopore and two reservoirs are filled with incompressible electrolyte solution containing  $M$  types of ionic species. PE brushes, referred to as PE layer, of uniform thickness  $h_m$  are end-grafted to the entire membrane wall surface. We assume that the PE layer is ion-penetrable and homogeneously structured. For simplicity, the morphology deformation of the PE layer is neglected, which is valid if the length of polymer chains is not too long.<sup>35</sup> Due to the axial symmetry, the cylindrical coordinate system,  $r$  and  $z$ , is adopted with the origin located at the center of the nanopore.

It is known that molecular chains in biological systems generally reveal a pH regulation nature, implying that their charges are exquisitely dependent on the local concentration of protons. To mimic the pH-regulated nature of biological ion channels, we assume that the PE brushes carry zwitterionic functional groups (e.g., lysine), PE~COOH and PE~NH<sub>2</sub>, capable of proceeding the following dissociation/association reactions:



Let  $K_A = \Gamma_{\text{PE}\sim\text{COO}^-}[\text{H}^+]/\Gamma_{\text{PE}\sim\text{COOH}}$  and  $K_B = \Gamma_{\text{PE}\sim\text{NH}_3^+}/\Gamma_{\text{PE}\sim\text{NH}_2}[\text{H}^+]$  be the equilibrium constants of these two reactions, where  $[\text{H}^+]$  and  $\Gamma_k$  are, respectively, the molar concentration of H<sup>+</sup> ions and the volume site densities of the functional groups  $k$  ( $k = \text{PE}\sim\text{COOH}, \text{PE}\sim\text{COO}^-, \text{PE}\sim\text{NH}_2$  and  $\text{PE}\sim\text{NH}_3^+$ ) within the PE layer. The total number concentrations of the acidic and basic functional groups are  $\Gamma_A = \Gamma_{\text{PE}\sim\text{COO}^-} + \Gamma_{\text{PE}\sim\text{COOH}} = \sigma_m / h_m$  and  $\Gamma_B = \Gamma_{\text{PE}\sim\text{NH}_3^+} + \Gamma_{\text{PE}\sim\text{NH}_2} = \sigma_m / h_m$ , respectively, with  $\sigma_m$  being the grafting density of PE chains on the membrane surface.  $\sigma_m$  is typically in the range of 0.1 and 0.6 chains/nm<sup>2</sup>.<sup>28,</sup>

<sup>29</sup> If we let  $e$  be the elementary charge, eqn (1) and the above relations of  $\Gamma_A$  and  $\Gamma_B$  yield the charge density of the PE layer,

$$\rho_m = 10^{27} e \left( -\Gamma_{\text{PE}\sim\text{COO}^-} + \Gamma_{\text{PE}\sim\text{NH}_3^+} \right) = 10^{27} e \left( -\frac{K_A \Gamma_A}{K_A + [\text{H}^+]} + \frac{K_B \Gamma_B [\text{H}^+]}{1 + K_B [\text{H}^+]} \right). \quad (2)$$

Suppose that the two reservoirs are large enough so that the concentration of the  $j$ th ionic species at positions far away from the nanopore maintains its bulk value,  $C_{j0}$  (mM). To simulate experimental conditions, we assume that the background salt is KCl, and HCl and

KOH are used to adjust the solution pH ( $= -\log[\text{H}^+]_0$ ) with  $[\text{H}^+]_0$  being the bulk molar concentration of  $\text{H}^+$  (in the unit of M). Therefore, four ionic species (i.e.,  $M = 4$ ), including  $\text{H}^+$ ,  $\text{K}^+$ ,  $\text{Cl}^-$ , and  $\text{OH}^-$ , should be considered. If we let  $C_{j0}$ ,  $j = 1, 2, 3$ , and 4, be the bulk concentrations of these ions, respectively, and  $C_b$  the background KCl concentration, electroneutrality results in  $C_{10} = 10^{-\text{pH}+3}$ ,  $C_{40} = 10^{-(14-\text{pH})+3}$ ,  $C_{20} = C_b$ , and  $C_{30} = C_b + 10^{-\text{pH}+3} - 10^{-(14-\text{pH})+3}$  for  $\text{pH} \leq 7$ ;  $C_{20} = C_b - 10^{-\text{pH}+3} + 10^{-(14-\text{pH})+3}$  and  $C_{30} = C_b$  for  $\text{pH} > 7$ .

The following verified continuum-based model,<sup>13, 30, 32, 36</sup> taking into account the presence of multiple ionic species,<sup>32</sup> is employed to describe the physics of the electrokinetic ion and fluid transport in nanopores:

(i) Multi-ion Poisson-Nernst-Planck (PNP) equations for the electrical potential  $V$  and the ionic mass transport:

$$-\nabla^2 V = \frac{\rho_e + i\rho_m}{\varepsilon_f}, \quad (3)$$

$$\nabla \cdot \mathbf{N}_j = \nabla \cdot \left( \mathbf{u}c_j - D_j \nabla c_j - z_j \frac{D_j}{RT} F c_j \nabla V \right) = 0, \quad j = 1, 2, 3, \text{ and } 4. \quad (4)$$

Here,  $\rho_e = \sum_{j=1}^4 F z_j c_j$  is the space charge density of mobile ions;  $z_j$ ,  $c_j$ ,  $D_j$ , and  $\mathbf{N}_j$  are the valence, concentration, diffusivity, and ionic flux of the ionic species of  $j$ , respectively;  $\varepsilon_f$  and  $T$  are the permittivity and absolute temperature of fluid, respectively;  $R$  and  $F$  are the universal gas constant and Faraday constant, respectively;  $\mathbf{u} = u_r \mathbf{e}_r + u_z \mathbf{e}_z$

is the fluid velocity with  $\mathbf{e}_r$  and  $\mathbf{e}_z$  being the unit vectors in the  $r$ - and  $z$ -directions, respectively;  $i=1$  and  $0$  are the regions inside and outside the PE layer, respectively. Note that the aforementioned PNP equations could not be replaced by the Poisson-Boltzmann equation<sup>37,38</sup> because the EDLs in the considered system are strongly overlapped and the ICP effect is significant.

(ii) Modified Stokes-Brinkman and continuity equations for the flow field:

$$\mu \nabla^2 \mathbf{u} - \nabla p - \left( \sum_{j=1}^4 F z_j c_j \right) \nabla V - i \frac{\mu}{\lambda_m^2} \mathbf{u} = \mathbf{0}, \quad (5)$$

$$\nabla \cdot \mathbf{u} = 0. \quad (6)$$

Here,  $\mu$  and  $p$  are the fluid viscosity and hydrodynamic pressure, respectively;  $\lambda_m = (\mu / \gamma_m)^{1/2}$  is the softness degree of the PE layer with  $\gamma_m$  being the hydrodynamic frictional coefficient of that layer.<sup>39</sup> Because the ionic current in nanopores is not significantly affected by the flow field,<sup>13,31,38</sup> in the present study  $\lambda_m$  is fixed at 1 nm, which is typical to biological PEs (ca. 0.1-10 nm).<sup>40</sup>

The following boundary conditions are assumed for the above highly coupled governing eqn (3)-(6). (i) The ionic concentrations on both ends of two reservoirs attain their bulk values,  $c_j = C_{j0}$ , and the corresponding electric potentials are  $V(\text{cathode}) = 0$  and  $V(\text{anode}) = V_0$ . A normal flow without external pressure gradient is specified on both ends of two reservoirs. (ii) The rigid surface of the membrane wall is ion-impenetrable, uncharged, and non-slip yielding  $\mathbf{n} \cdot \mathbf{N}_j = 0$ ,  $-\mathbf{n} \cdot \nabla V = 0$ , and  $\mathbf{u} = \mathbf{0}$ ,<sup>30</sup> respectively. Here  $\mathbf{n}$  is the unit

outer normal vector. (iii) The electric potential, electric field, ionic concentrations, and flow field are all continuous on the PE-layer/liquid interface. (iv) Zero normal ionic fluxes ( $\mathbf{n} \cdot \mathbf{N}_j = 0$ ), insulation boundary condition for the potential ( $-\mathbf{n} \cdot \nabla V = 0$ ), and slip boundary condition for the flow field are specified on the side boundaries of two reservoirs, which are far away from the nanopore. (v) Symmetric boundary condition is imposed along the axis of the nanopore.

The ion conductance and selectivity of the nanopore,  $G$  and  $S$ , respectively, can be evaluated by<sup>14, 36</sup>

$$G = I / V_0 = \left[ \int_{\Omega} \left( \sum_{j=1}^4 Fz_j \mathbf{N}_j \right) \cdot \mathbf{n} d\Omega \right] / V_0, \quad (7)$$

and

$$S = \frac{|I_{ca}| - |I_{an}|}{|I_{ca}| + |I_{an}|}. \quad (8)$$

In the above,  $\Omega$  denotes either end of two reservoirs, and  $I = |I_{ca}| + |I_{an}|$  is the net ionic current through the nanopore with  $I_{ca} = I_1 + I_2 = \int_{\Omega} \left( \sum_{j=1}^2 Fz_j \mathbf{N}_j \right) \cdot \mathbf{n} d\Omega$  from  $\text{H}^+$  and  $\text{K}^+$  ions and  $I_{an} = I_3 + I_4 = \int_{\Omega} \left( \sum_{j=3}^4 Fz_j \mathbf{N}_j \right) \cdot \mathbf{n} d\Omega$  from  $\text{Cl}^-$  and  $\text{OH}^-$  ions. If  $S > 0$  ( $S < 0$ ) and  $S = 0$ , implying that  $|I_{ca}| > |I_{an}|$  ( $|I_{ca}| < |I_{an}|$ ) and  $|I_{ca}| = |I_{an}|$ , the nanopore is cation-selective (anion-selective) and non-selective, respectively.

The above strongly coupled model is solved numerically by COMSOL Multiphysics (version 4.3a), operated in a high-performance cluster. The model without considering the charge regulation and multiple ionic species has been validated to be sufficiently efficient and

accurate for quantitatively describing similar electrokinetic ion transport problems in solid-state<sup>13, 14, 41-43</sup> and PE-modified nanopores.<sup>30, 33</sup> The applicability of the similar charge regulation model was also validated recently<sup>36</sup> by comparing the predicted conductance in a silica solid-state nanopore with the experimental data obtained by Smeets et al.<sup>44</sup> A more detailed description of the numerical implementation is available in the literature.<sup>25, 45</sup>

### 3. Results and Discussion

For illustration, we consider a PE layer-modified nanopore with radius  $R_n = 14$  nm and length  $L_n = 60$  nm, and the thickness of PE layer  $h_m = 5$  nm. The former is in accordance with the typical dimensions of nanopores drilled in solid-state membranes,<sup>46, 47</sup> and the latter is within the range for biological PE brushes<sup>8, 28, 47</sup> (ca. 3-15 nm) in the surface modification of nanopores. To simulate biomimetic nanopores with pH-tunable, zwitterionic characteristics, we consider a typical case of amino acid-like PE chains with lysine groups<sup>7, 8</sup> of  $pK_A = 2.2$  ( $\alpha$ -carboxyl) and  $pK_B = -9$  ( $\alpha$ -amino).<sup>48</sup> Consequently, the isoelectric point (IEP) of the PE layer is 5.6. At  $T = 298$  K, the ionic diffusivities  $D_1$  ( $H^+$ ),  $D_2$  ( $K^+$ ),  $D_3$  ( $Cl^-$ ), and  $D_4$  ( $OH^-$ ) are 9.31, 1.96, 2.03, and  $5.30 (\times 10^{-9} \text{ m}^2 / \text{s})$ , respectively,<sup>21</sup> and the other physical parameters are  $F = 96490$  C/mol,  $R = 8.31 \text{ JK}^{-1} \text{ mol}^{-1}$ ,  $\varepsilon_f = 7.08 \times 10^{-10}$  F/m, and  $\mu = 1 \times 10^{-3}$  Pa·s.

#### 3.1. Nanopore conductance

The influences of the solution pH, background KCl concentration,  $C_b$ , grafting density of PE chains on the membrane surface,  $\sigma_m$ , and voltage bias,  $V_0$ , on the nanopore conductance,  $G$ , are depicted in Fig. 2. Fig. 2a and b reveal that at sufficiently high salt concentration,  $G$  is nearly independent of  $V_0$ , pH, and  $\sigma_m$ , and decreases linearly with decreasing  $C_b$ . This, as expected, behaves as a bulk conductance behavior. On the contrary,  $G$  decreases non-linearly with a decrease in  $C_b$  at low regime of salt concentration. This is due to the fact that at low salt concentration, the overlapping of electric double layers (EDLs) in the nanopore is significant. In this case, the nanopore conductance is primarily dominated by its surface charges.<sup>49, 50</sup> This explains why the non-linear conductance behavior at small  $\sigma_m = 0.1$  and medium small pH = 5 (close to IEP of the considered PE layer), shown in Fig. 2a, is unremarkable, as a result of a very small charge density of the PE layer. Because the amount of charges in the PE layer increases with an increase in  $\sigma_m$ , the nanopore conductance increases accordingly, as shown in Fig. 2b.

Fig. 2c and d reveal that  $G$  shows a local minimum as pH varies; that is, the larger the deviation of pH from the IEP of PE layer, the larger is the nanopore conductance. This stems from the following two reasons: (i) the ionic strength of aqueous solution increases with the deviation of pH from neutrality, and (ii) the more acidic (basic) environments, the more amount of  $\text{PE}\sim\text{NH}_3^+$  ( $\text{PE}\sim\text{COO}^-$ ) formed from the considered zwitterionic PE brushes and, therefore, the larger charge density of PE layer. As explained previously, because at low salt

concentration, the charge property of a nanopore primarily affects its conductance behavior, the dependence of  $G$  on pH is more significant at lower salt concentration (e.g.,  $C_b = 1 \text{ mM}$ ) and higher  $\sigma_m = 0.5$ , as shown in Fig. 2d.

It is interesting to note in Fig. 2 that the ionic conductance in the pH tunable, PE layer-modified nanopore is dependent on the levels of voltage bias,  $V_0$ , and such dependence is related to the values of  $\sigma_m$ , pH, and  $C_b$ . For example, if pH is apparently lower than the IEP of PE layer (5.6), the nanopore conductance for  $V_0 = 1 \text{ V}$  (symbols) is smaller than that for  $V_0 = 0.2 \text{ V}$  (lines) regardless of the values of  $\sigma_m$ , pH, and  $C_b$ . If pH is close to the IEP of PE layer, the nanopore conductance is nearly independent of  $V_0$ . If pH is apparently higher than the IEP of PE layer, the nanopore conductance for  $V_0 = 1 \text{ V}$  (symbols) is larger than that for  $V_0 = 0.2 \text{ V}$  (lines) when  $\sigma_m$  is small, pH is medium and extremely high, or  $C_b$  is relatively high; however, the reverse trend is observed at sufficiently large  $\sigma_m$ , high pH, and low  $C_b$ , as shown in Fig. 2b and d. As pointed out by Yeh et al.<sup>33</sup> in the study of the ion concentration polarization (ICP) in the nanopore modified with a fixed charge density of PE layer, the  $V_0$ -dependence of the nanopore conductance behavior is highly related to its ICP behaviors. Typically, if  $V_0$  is not very large, the more serious the ICP phenomenon, which is significant at the condition of significant EDL overlapping (e.g., at low salt concentration) and for nanopores with high surface charges, the smaller is the nanopore conductance at relatively larger  $V_0$ . This is because as  $V_0$  increases, the movement of ions

through a nanopore will be electrostatically obstructed by an appreciable enrichment of ions at one side of the nanopore due to the significant ICP effect. As a result, the rate of increase in the ionic fluxes with increasing  $V_0$  is smaller than that of increase in  $V_0$ , leading to a smaller nanopore conductance at larger  $V_0$ . In the present case, if pH is close to the IEP of PE layer, the ICP effect, due to a small charge density of PE layer, is insignificant, so that the nanopore conductance is nearly independent of  $V_0$ . Moreover, if pH is apparently higher than the IEP of PE layer, the PE layer-modified nanopore is negatively charged and attracts counterions ( $H^+$  and  $K^+$ ) inside the nanopore. Note that an attraction of  $H^+$  ions results in an increase in the local concentration of protons inside the PE layer and, therefore, a decrease in its charge density. As a consequence, a larger  $\sigma_m$ , sufficiently higher pH, and lower  $C_b$  are required to induce a more significant ICP effect, as schematically shown in Fig. 3a, and, therefore, a smaller nanopore conductance for larger  $V_0$ . Note in Fig. 2d that if pH is extremely high, the nanopore conductance for  $V_0 = 1\text{ V}$  becomes larger than that for  $V_0 = 0.2\text{ V}$ . This is because the overlapping of EDLs in the PE layer-modified nanopore becomes less significant, and so does the ICP effect, due to an appreciable increase in the ionic strength from  $OH^-$  ions.

It is worth noting that if pH is apparently lower than the IEP of PE layer (5.6), the charge density of PE layer is positive, which makes coions, including  $H^+$  and  $K^+$  ions, difficult to migrate through the nanopore. Furthermore, the proton concentration at low pH is

comparably high. In this case, even though a portion of  $H^+$  ions is capable of being electrokinetically driven into the nanopore, yielding a higher local proton concentration inside the PE layer, the charge density of PE layer hence becomes large. This prevents more protons migrating through the nanopore, and results in an apparently uneven distribution of protons between the nanopore and reservoirs, and, therefore, a significant ICP effect, as schematically shown in Fig. 3b. In this case, the nanopore conductance also becomes smaller for larger  $V_0$ .

### 3.2. Ion concentration polarization

To further understand the ICP phenomenon in the pH-tunable, PE layer-modified nanopore, Fig. 4 illustrates the influence of pH on the spatial variations of the cross-section-averaged concentrations of  $H^+$  ions,  $c_{a1}$ , net cations,  $c_{a1} + c_{a2}$ , and net anions,  $c_{a3} + c_{a4}$ , at  $\sigma_m = 0.1$  chains/nm<sup>2</sup> and  $C_b = 1$  mM, and the influences of  $\sigma_m$  and  $C_b$  at pH = 10 are shown in Fig. 5. As schematically shown in Fig. 3b, if pH < 5.6 (the IEP of the considered PE layer), the PE layer-modified nanopore is positively charged, thus attracting counterions ( $Cl^-$  and  $OH^-$ ) into and repelling coions ( $H^+$  and  $K^+$ ) out of the nanopore. In this case, the ionic flux of cations (anions) inside the nanopore is depleted (enriched), while that at both reservoirs is enriched (depleted). Because  $\mathbf{J}_{np}^+ \ll \mathbf{J}_{ca}^+$ ,  $\mathbf{J}_{np}^+ \ll \mathbf{J}_{an}^+$ ,  $\mathbf{J}_{np}^- \gg \mathbf{J}_{ca}^-$ , and  $\mathbf{J}_{np}^- \gg \mathbf{J}_{an}^-$ , the ICP effect yields an enrichment (a depletion) of  $H^+$  ions, net cations, and net anions near the anode (cathode) side of the nanopore, as shown

in Fig. 4a-d. Because the charge density of PE layer increases with the deviation of pH from its IEP, the PE layer-modified nanopore carries more positive charges at lower pH = 2.2 compared to pH = 5, leading to a more significant exclusion of H<sup>+</sup> ions outside the nanopore and, therefore, ICP phenomenon (Fig. 4a-b). Fig. 4a-b also reveals that the larger the  $V_0$ , the more significant the ICP effect. This can be attributed to the same reason of a significant exclusion effect of H<sup>+</sup> ions by the PE layer-modified nanopore with positive and high charges as mentioned previously.

On the other hand, if pH > 5.6, the PE layer-modified nanopore becomes negatively charged, leading to more counterions (H<sup>+</sup> and K<sup>+</sup>) attracted into and coions (Cl<sup>-</sup> and OH<sup>-</sup>) repelled outside the nanopore. In this case,  $\mathbf{J}_{np}^+ \gg \mathbf{J}_{ca}^+$ ,  $\mathbf{J}_{np}^+ \gg \mathbf{J}_{an}^+$ ,  $\mathbf{J}_{np}^- \ll \mathbf{J}_{ca}^-$ , and  $\mathbf{J}_{np}^- \ll \mathbf{J}_{an}^-$ . Therefore, the concentrations of H<sup>+</sup> ions, net cations, and net anions are enriched (depleted) near the cathode (anode) side of the nanopore, as shown in Fig. 4e-f and 5, and schematically depicted in Fig. 3a. To estimate the significance of the ICP effect, we define two parameters,  $f^+ = \left[ (c_{a1} + c_{a2})_{\max} - (c_{a1} + c_{a2})_{\min} \right] / C_b$  and  $f^- = \left[ (c_{a3} + c_{a4})_{\max} - (c_{a3} + c_{a4})_{\min} \right] / C_b$ , where  $(c_{a1} + c_{a2})_{\max}$  and  $(c_{a1} + c_{a2})_{\min}$  ( $(c_{a3} + c_{a4})_{\max}$  and  $(c_{a3} + c_{a4})_{\min}$ ) are, respectively, the maximum and minimum values of the polarized cross-section-averaged concentrations of net cations (anions) along the axis of the nanopore. The larger the value of  $f^+$  ( $f^-$ ) represents the more significant the concentration polarization of cations (anions). In Fig. 4b at pH = 2.2 (4f at pH = 9), the

values of  $f^+$  and  $f^-$  are, respectively, 4.00 and 6.41 (3.24 and 0.95) for  $V_0 = 0.2$  V, and 7.00 and 11.40 (3.97 and 1.51) for  $V_0 = 1$  V. This implies that even though the deviations of the solution pH from the IEP of PE layer (pH = 5.6) in Fig. 4b (pH = 2.2) and 4f (pH = 9) are the same, the ICP phenomenon in the former is apparently more significant than that in the latter regardless of the levels of  $V_0$ . In addition, with  $V_0$  increasing from 0.2 to 1 V, the degree of ICP phenomenon at lower pH = 2.2 becomes more appreciable than that at higher pH = 9. This explains why the nanopore conductance decreases with an increase in  $V_0$  at relatively low pH, as shown in Fig. 2.

Fig. 5 shows the typical ICP phenomenon for a negatively charged nanopore, in which the ionic concentrations are enhanced near its cathode side, while reduced near anode side. Comparison between Fig. 5a,b ( $\sigma_m = 0.1$  chains/nm<sup>2</sup>) and 5c,d ( $\sigma_m = 0.5$  chains/nm<sup>2</sup>) reveals that the larger the grafting density of PE chains on the membrane wall, the more significant the ICP phenomenon. This is expected because the charge density of PE layer increases with an increase in  $\sigma_m$ . In Fig. 5b at  $\sigma_m = 0.1$  chains/nm<sup>2</sup> (5d  $\sigma_m = 0.5$  chains/nm<sup>2</sup>), the values of  $f^+$  and  $f^-$  are, respectively, 9.00 and 1.42 (23.98 and 1.88) for  $V_0 = 0.2$  V, and 10.81 and 3.60 (25.74 and 6.43) for  $V_0 = 1$  V. This implies that as  $V_0$  increases, the enhancement of ICP phenomenon is more remarkable for larger  $\sigma_m = 0.5$  chains/nm<sup>2</sup>. As obtained from Fig. 5f, the values of  $f^+$  and  $f^-$  are, respectively, 0.75 and 0.49 for  $V_0 = 0.2$  V, and 1.53 and 1.14 for  $V_0 = 1$  V. Comparing the values of  $f^+$  and  $f^-$

between Fig. 5d and f clearly reveals that the ICP phenomenon becomes less significant as  $C_b$  increases. This stems from the fact that the higher the salt concentration the thinner the EDL thickness and, therefore, the less significant the degree of ICP.

Fig. 6 and 7 illustrate the influences of pH,  $\sigma_m$ , and  $C_b$  on the spatial variations of the charge density of PE layer,  $\rho_m$ , in the considered biomimetic nanopores at two levels of  $V_0$ . As described in eqn (2),  $\rho_m$  is dependent on the local proton concentration inside the PE layer. As shown in Fig. 3a, c, e, and 4a, c, e, because the variations of protons along the axis of the nanopore at various conditions of pH,  $\sigma_m$ ,  $C_b$ , and  $V_0$  are different, the charge density of PE layer varies accordingly. For example, if  $\text{pH} < 5.6$  ( $\text{pH} > 5.6$ ), the considered biomimetic nanopore, as expected, is positively (negatively) charged, and the magnitude of the charge density of PE layer near the cathode side of the nanopore is smaller (larger) than its anode side, as shown in Fig. 6a and 7a (6b-d and 7b-d). Apparently, these behaviors arise from the concentration polarization of  $\text{H}^+$  ions in the nanopores with different polarities of charged nature depicted in Fig. 3a, c, e, and 4a, c, e.

Fig. 6b-d and 7b-d also suggests that the larger the grafting density on the membrane wall and the lower the background salt concentration, the more significant the uneven distribution of  $\rho_m$ . This can be attributed to the more significant ICP phenomenon at larger  $\sigma_m$  and lower  $C_b$ . Comparison between Fig. 6 and 7 shows that since the ICP phenomenon is more appreciable at larger  $V_0$ ,  $\rho_m$  becomes more unevenly distributed. These results clearly

indicate that the assumption of homogeneously fixed charge density of PE layer<sup>28-30, 32, 33, 51-53</sup> is inappropriate and might result in an incorrect estimation for the ion transport in such soft nanofluidics with a surface modification of PE brushes.

### 3.3. Ion selectivity

Fig. 8 summarizes the influences of pH,  $\sigma_m$ , and  $C_b$  on the ion selectivity,  $S$ , in the considered biomimetic PE layer-modified nanopore at two levels of  $V_0$  (lines for  $V_0 = 0.2$  V and symbols for  $V_0 = 1$  V). In this figure, if  $S > 0$  ( $S < 0$ ), the more significant deviation of  $S$  from 0 represents the more significant cation-selective (anion-selective), implying that the ionic current (or ionic flux) arising from cations (anions) is larger than that from anions (cations). Fig. 8 reveals that if pH is higher than the IEP of PE layer (5.6), the considered biomimetic nanopore generally shows cation-selective ( $S > 0$ ) and its ion selectivity,  $S$ , decreases with an increase in  $C_b$  except when  $V_0$  and pH are sufficiently high. The former is expected since the nanopore is negatively charged at pH higher than 5.6. The latter can be attributed to the less significant overlapping of EDLs in a nanopore. It is worth noting in Fig. 8c and d that if  $V_0$  is sufficiently large, implying that the axially applied electric field is sufficiently large to disturb the equilibrium one stemming from the EDLs in the nanopore, the ion selectivity of the nanopore for smaller  $C_b$  is smaller than that for higher  $C_b$  and is even reversed from positive (cation-selective) to negative (anion-selective) at sufficiently high pH. This can be attributed to the significantly richer  $\text{OH}^-$  ions in the

entire composition of bulk solution at relatively higher pH and lower background salt concentration. Because the ionic mobility of  $\text{OH}^-$  is apparently larger than the other two background salt ions ( $\text{K}^+$  and  $\text{Cl}^-$ ), a comparable enhancement of  $\text{OH}^-$  ions in bulk solution results in an increase in the ionic current from anions ( $|I_{an}|$ ) and might dominate the ion selectivity of the nanopore. Consequently, the negatively charged nanopore becomes less cation-selective at extremely high pH (i.e.,  $S$  shows a local maximum as pH increases) and even turns into anion-selective at sufficiently low  $C_b$  and large  $V_0$ .

It is interesting to note in Fig. 8 that if pH is lower than the IEP of PE layer the ion selectivity of the considered biomimetic nanopore depends on the levels of pH,  $\sigma_m$ ,  $C_b$ , and  $V_0$ . For example, the nanopore reveals anion-selective ( $S < 0$ ) when  $\sigma_m$  is sufficiently large (Fig. 8d), pH is slightly lower than 5.6 (Fig. 8a and c), or  $C_b$  is sufficiently high (inset in Fig. 8a), while cation-selective ( $S > 0$ ) when the values of  $\sigma_m$ , pH, and  $C_b$  are sufficiently small (Fig. 8a and c). The selectivity of anions for a positively charged nanopore is expected. The apparent reverse of the ion selectivity for a positively charged nanopore is unexpected and has not been reported previously. Because the concentration of  $\text{H}^+$  ions, which have greater ionic mobility than other three ionic species, becomes higher at relatively lower solution pH, its transport phenomenon might dominate the ion selectivity behavior in the nanopore. As pH decreases, an increase in the concentration of  $\text{H}^+$  ions leads to an increase in the ionic current from cations ( $|I_{ca}|$ ) and then the selectivity of cations (i.e., an increase in

$S$ ). Note that this effect is significant when  $\sigma_m$  is small,  $C_b$  is low, and  $V_0$  is large. This is because the smaller the value of  $\sigma_m$  the smaller the charge density of PE layer (or equilibrium electric field) and the larger the value of  $V_0$  the stronger the axial local electric field in the nanopore. Therefore, it is easier for enriched cations to pass through the nanopore, thus leading to an increase in  $S$ . Furthermore, the lower the  $C_b$ , the richer the composition of  $H^+$  ions in bulk solution, dominating the ion selectivity of a nanopore. This clearly explains why the ion selectivity of the considered biomimetic nanopore is reversed from anion-selective to cation-selective at sufficiently small values of  $\sigma_m$ , pH, and  $C_b$ .

#### 4. Conclusions

The electrokinetic ion transport in a pH-tunable, biomimetic polyelectrolyte (PE) layer-modified nanopore connecting two large reservoirs, a typical bioinspired device widely used in modern nanotechnology, is studied theoretically for the first time. To mimic the pH-regulated nature in biological systems, the developed model extends the existing ones, where the charge density of PE layer is assumed to be a constant and only the background salt ions are considered, to a more general case with consideration of the presence of  $H^+$  and  $OH^-$  ions and the interfacial chemistry reactions on PE chains. The model predicts that the charge density of PE layer in the nanopore is pH-dependent, and spatially dependent due to the different degrees of ion concentration polarization (ICP) effect at various values of the

background salt concentration, pH, grafting density of PE chain, and applied voltage bias, thus leading to many interesting and unexpected ion transport phenomena. For example, if pH is apparently lower than the isoelectric point (IEP) of PE layer, the ionic conductance in the nanopore for larger voltage bias is larger than that for smaller voltage only when the grafting density of PE chains is small and the background salt concentration is sufficiently high. However, if pH is apparently higher than the IEP of PE layer, the nanopore conductance for larger voltage bias turns into smaller than that for smaller voltage regardless of the levels of grafting density of PE chains and background salt concentration. We also show that the tuning of ion selectivity in the biomimetic nanopore from anion-selective (cation-selective) to cation-selective (anion-selective) by decreasing (increasing) the solution pH under the conditions of a sufficiently small grafting density of PE chains, large voltage bias, and low background salt concentration. The results provide valuable information for constructing smart nanopore systems, which show great promise in many applications, including ionic gates/diodes, energy conversion, and single-molecule biosensing.

### **Acknowledgements**

This work is supported, in part, by the Ministry of Science and Technology of the Republic of China under Grants 102-2221-E-224-052-MY3 and 103-2221-E-224-039-MY3 (L.H.Y.), and the State Scholarship Fund of China under Grant No. 2011684502 (Z.Z.).

**References**

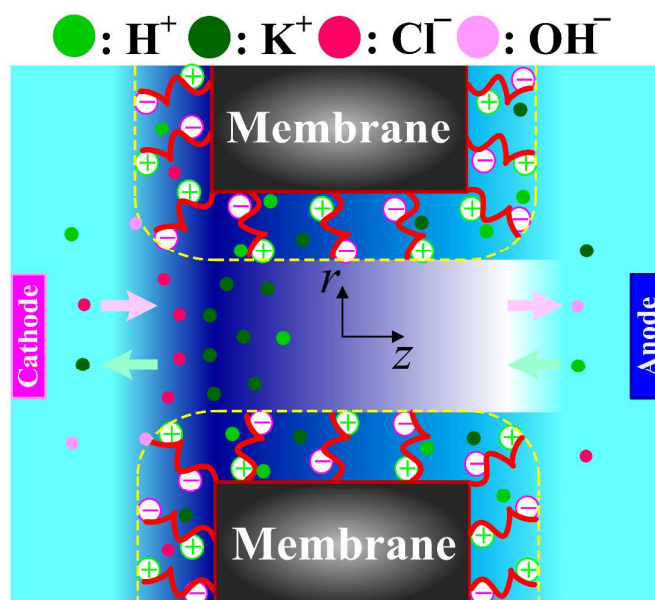
1. L. P. Wen, Y. Tian, J. Ma, J. Zhai and L. Jiang, *Phys. Chem. Chem. Phys.*, 2012, **14**, 4027-4042.
2. X. Hou, Y. J. Liu, H. Dong, F. Yang, L. Li and L. Jiang, *Adv. Mater.*, 2010, **22**, 2440-2443.
3. S. F. Buchsbaum, G. Nguyen, S. Howorka and Z. S. Siwy, *J. Am. Chem. Soc.*, 2014, **136**, 9902-9905.
4. H. C. Zhang, X. Hou, J. Hou, L. Zeng, Y. Tian, L. Li and L. Jiang, *Adv. Funct. Mater.*, 2015, **25**, 1102-1110.
5. B. Yameen, M. Ali, R. Neumann, W. Ensinger, W. Knoll and O. Azzaroni, *Nano Lett.*, 2009, **9**, 2788-2793.
6. H. C. Zhang, X. Hou, L. Zeng, F. Yang, L. Li, D. D. Yan, Y. Tian and L. Jiang, *J. Am. Chem. Soc.*, 2013, **135**, 16102-16110.
7. M. Ali, P. Ramirez, S. Mafe, R. Neumann and W. Ensinger, *ACS Nano*, 2009, **3**, 603-608.
8. B. Yameen, M. Ali, R. Neumann, W. Ensinger, W. Knoll and O. Azzaroni, *J. Am. Chem. Soc.*, 2009, **131**, 2070-2071.
9. L. Lin, J. Yan and J. H. Li, *Anal. Chem.*, 2014, **86**, 10546-10551.
10. W. Guo, H. W. Xia, L. X. Cao, F. Xia, S. T. Wang, G. Z. Zhang, Y. L. Song, Y. G. Wang, L. Jiang and D. B. Zhu, *Adv. Funct. Mater.*, 2010, **20**, 3561-3567.
11. Q. Liu, K. Xiao, L. P. Wen, Y. Dong, G. H. Xie, Z. Zhang, Z. S. Bo and L. Jiang, *ACS Nano*, 2014, **8**, 12292-12299.
12. M. H. Zhang, X. Hou, J. T. Wang, Y. Tian, X. Fan, J. Zhai and L. Jiang, *Adv. Mater.*, 2012, **24**, 2424-2428.
13. I. Vlassiouk, S. Smirnov and Z. Siwy, *Nano Lett.*, 2008, **8**, 1978-1985.
14. L. H. Yeh, C. Hughes, Z. Zeng and S. Qian, *Anal. Chem.*, 2014, **86**, 2681-2686.
15. C. C. Chang, C. P. Yeh and R. J. Yang, *Electrophoresis*, 2012, **33**, 758-764.
16. H. Jeon, H. Lee, K. H. Kang and G. Lim, *Sci. Rep.*, 2013, **3**, 3483.

17. M. Jia and T. Kim, *Anal. Chem.*, 2014, **86**, 7360-7367.
18. Z. S. Siwy, *Adv. Funct. Mater.*, 2006, **16**, 735-746.
19. J. Liu, D. C. Wang, M. Kvetny, W. Brown, Y. Li and G. L. Wang, *Langmuir*, 2013, **29**, 8743-8752.
20. S. Nasir, M. Ali, P. Ramirez, V. Gomez, B. Oschmann, F. Muench, M. N. Tahir, R. Zentel, S. Mafe and W. Ensinger, *ACS Appl. Mater. Interfaces*, 2014, **6**, 12486-12494.
21. Y. Ma, L. H. Yeh and S. Qian, *Electrochem. Commun.*, 2014, **43**, 91-94.
22. Y. Ma, L. H. Yeh, C. Y. Lin, L. J. Mei and S. Z. Qian, *Anal. Chem.*, 2015, **87**, 4508-4514.
23. J. T. Wang, M. H. Zhang, J. Zhai and L. Jiang, *Phys. Chem. Chem. Phys.*, 2014, **16**, 23-32.
24. Y. C. Chung, J. P. Hsu and S. Tseng, *J. Phys. Chem. C*, 2014, **118**, 19498-19504.
25. Y. Ai, M. K. Zhang, S. W. Joo, M. A. Cheney and S. Qian, *J. Phys. Chem. C*, 2010, **114**, 3883-3890.
26. X. Kong, J. Jiang, D. N. Lu, Z. Liu and J. Z. Wu, *J. Phys. Chem. Lett.*, 2014, **5**, 3015-3020.
27. D. H. Lin, C. Y. Lin, S. Tseng and J. P. Hsu, *Nanoscale*, 2015, **7**, 14023-14031.
28. M. Tagliazucchi, Y. Rabin and I. Szleifer, *J. Am. Chem. Soc.*, 2011, **133**, 17753-17763.
29. M. Tagliazucchi, Y. Rabin and I. Szleifer, *ACS Nano*, 2013, **7**, 9085-9097.
30. L. H. Yeh, M. Zhang, N. Hu, S. W. Joo, S. Qian and J. P. Hsu, *Nanoscale*, 2012, **4**, 5169-5177.
31. L. H. Yeh, M. Zhang, S. Qian and J. P. Hsu, *Nanoscale*, 2012, **4**, 2685-2693.
32. L. H. Yeh, M. K. Zhang, S. W. Joo, S. Qian and J. P. Hsu, *Anal. Chem.*, 2012, **84**, 9615-9622.
33. L. H. Yeh, M. Zhang, S. Qian, J. P. Hsu and S. Tseng, *J. Phys. Chem. C*, 2012, **116**, 8672-8677.
34. Z. Zeng, Y. Ai and S. Qian, *Phys. Chem. Chem. Phys.*, 2014, **16**, 2465-2474.

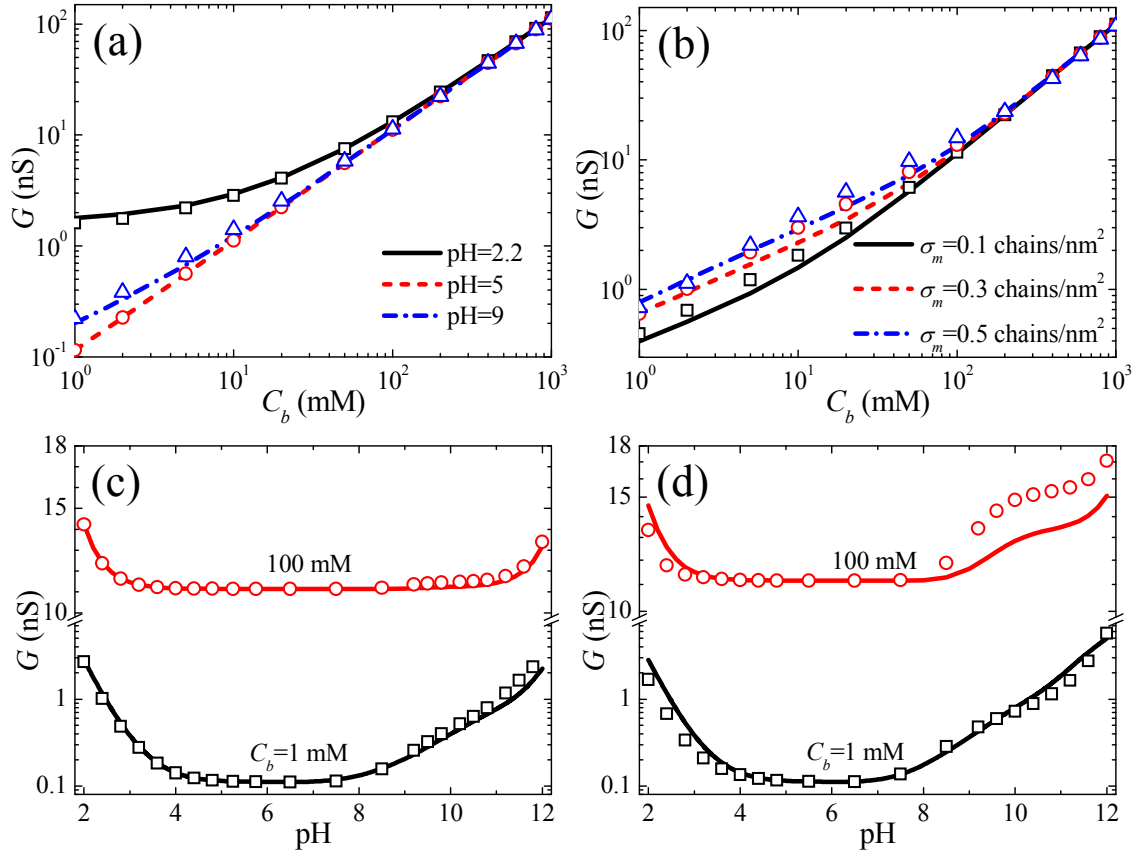
35. O. Peleg, M. Tagliazucchi, M. Kroger, Y. Rabin and I. Szleifer, *ACS Nano*, 2011, **5**, 4737-4747.
36. L. H. Yeh, M. Zhang and S. Qian, *Anal. Chem.*, 2013, **85**, 7527-7534.
37. M. J. Huang, L. J. Mei, L. H. Yeh and S. Z. Qian, *Electrochem. Commun.*, 2015, **55**, 60-63.
38. Y. H. He, M. Tsutsui, C. Fan, M. Taniguchi and T. Kawai, *ACS Nano*, 2011, **5**, 5509-5518.
39. H. Ohshima, *Curr. Opin. Colloid Interface Sci.*, 2013, **18**, 73-82.
40. J. F. L. Duval and F. Gaboriaud, *Curr. Opin. Colloid Interface Sci.*, 2010, **15**, 184-195.
41. W. J. Lan, D. A. Holden and H. S. White, *J. Am. Chem. Soc.*, 2011, **133**, 13300-13303.
42. L. Luo, D. A. Holden, W. J. Lan and H. S. White, *ACS Nano*, 2012, **6**, 6507-6514.
43. N. Y. Sa, W. J. Lan, W. Q. Shi and L. A. Baker, *ACS Nano*, 2013, **7**, 11272-11282.
44. R. M. M. Smeets, U. F. Keyser, D. Krapf, M. Y. Wu, N. H. Dekker and C. Dekker, *Nano Lett.*, 2006, **6**, 89-95.
45. L. H. Yeh, M. Zhang, N. Hu, S. W. Joo, S. Qian and J. P. Hsu, *Nanoscale*, 2012, **4**, 5169-5177.
46. A. J. Storm, J. H. Chen, X. S. Ling, H. W. Zandbergen and C. Dekker, *Nat. Mater.*, 2003, **2**, 537-540.
47. E. C. Yusko, J. M. Johnson, S. Majd, P. Prangkio, R. C. Rollings, J. L. Li, J. Yang and M. Mayer, *Nat. Nanotechnol.*, 2011, **6**, 253-260.
48. R. Switzer and L. Garrity, *Experimental Biochemistry*, W. H. Freeman Publishing, New York, USA, 1999.
49. R. B. Schoch, J. Y. Han and P. Renaud, *Rev. Mod. Phys.*, 2008, **80**, 839-883.
50. Y. Ma, S. Xue, S. C. Hsu, L. H. Yeh, S. Qian and H. Tan, *Phys. Chem. Chem. Phys.*, 2014, **16**, 20138-20146.
51. L. Benson, L. H. Yeh, T. H. Chou and S. Qian, *Soft Matter*, 2013, **9**, 9767-9773.

52. G. Chen and S. Das, *J. Colloid Interface Sci.*, 2015, **445**, 357-363.
53. S. Chanda, S. Sinha and S. Das, *Soft Matter*, 2014, **10**, 7558-7568.

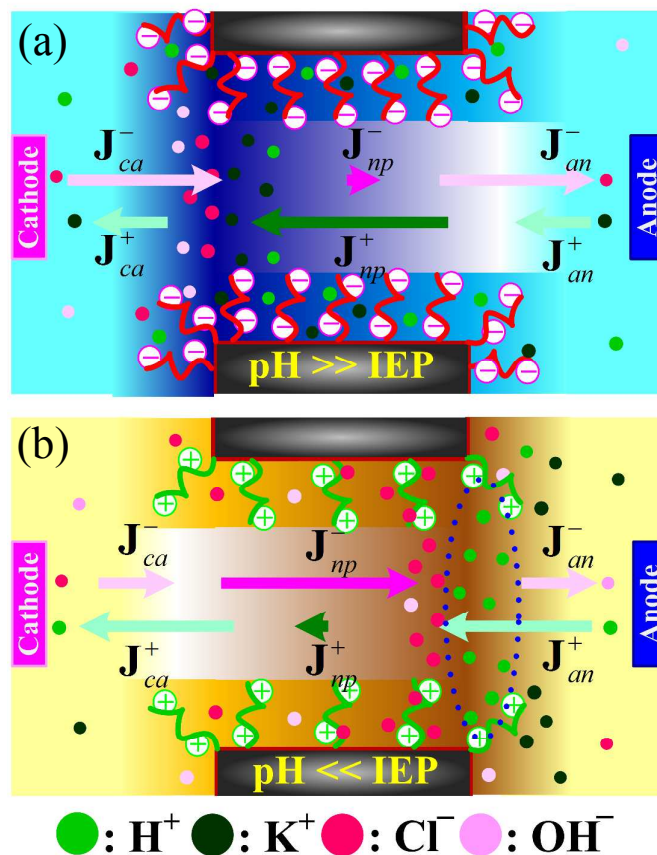
## Figure Captions



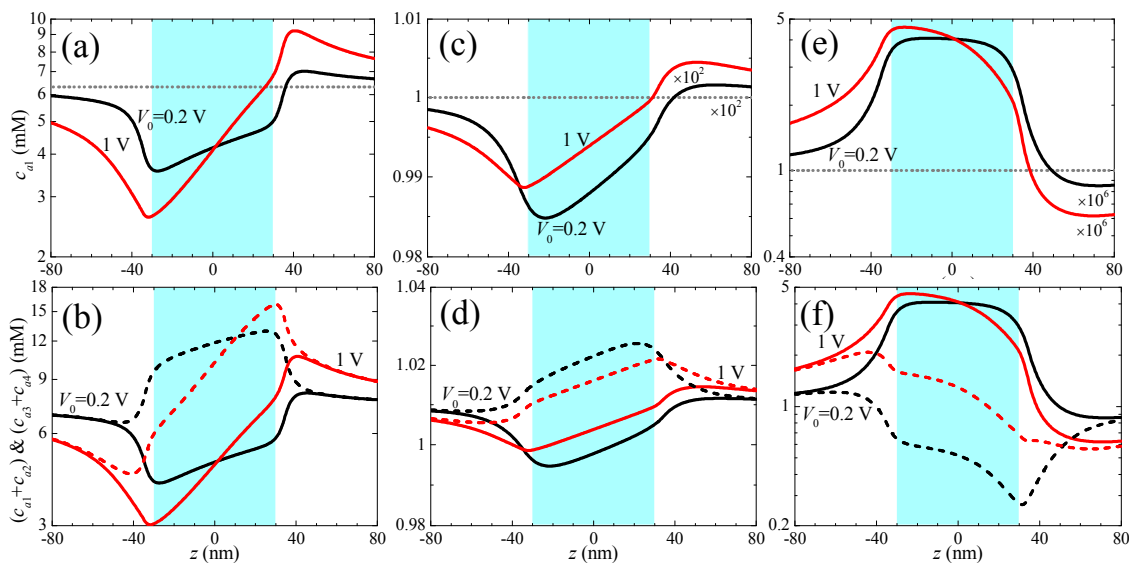
**Fig. 1.** Schematic of the ion transport in a pH-tunable, biomimetic PE layer-modified (e.g., negatively charged) nanopore filled with electrolyte solution containing four ionic species,  $\text{H}^+$ ,  $\text{K}^+$ ,  $\text{Cl}^-$ , and  $\text{OH}^-$ .



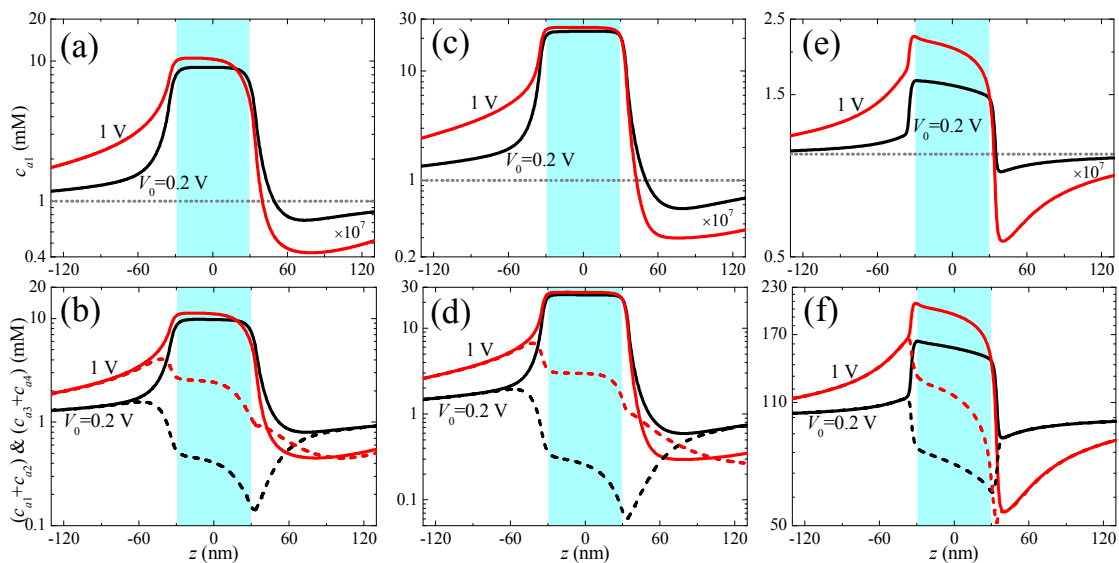
**Fig. 2.** Nanopore conductance  $G$  as a function of the background salt concentration  $C_b$  for various pHs at  $\sigma_m = 0.1$  chains/nm<sup>2</sup>, (a), and for various  $\sigma_m$  at pH = 10, (b), and as a function of pH for two levels of  $C_b$  at  $\sigma_m = 0.1$  chains/nm<sup>2</sup>, (c), and 0.5 chains/nm<sup>2</sup>, (d). Lines and symbols denote the results for  $V_0 = 0.2$  V and 1 V, respectively. “ $\square$ ”, “ $\circ$ ”, and “ $\triangle$ ” in (a) denote the results for pH = 2.2, 5, and 9, respectively, and in (b) denote the results for  $\sigma_m = 0.1, 0.3$ , and 0.5 chains/nm<sup>2</sup>, respectively.



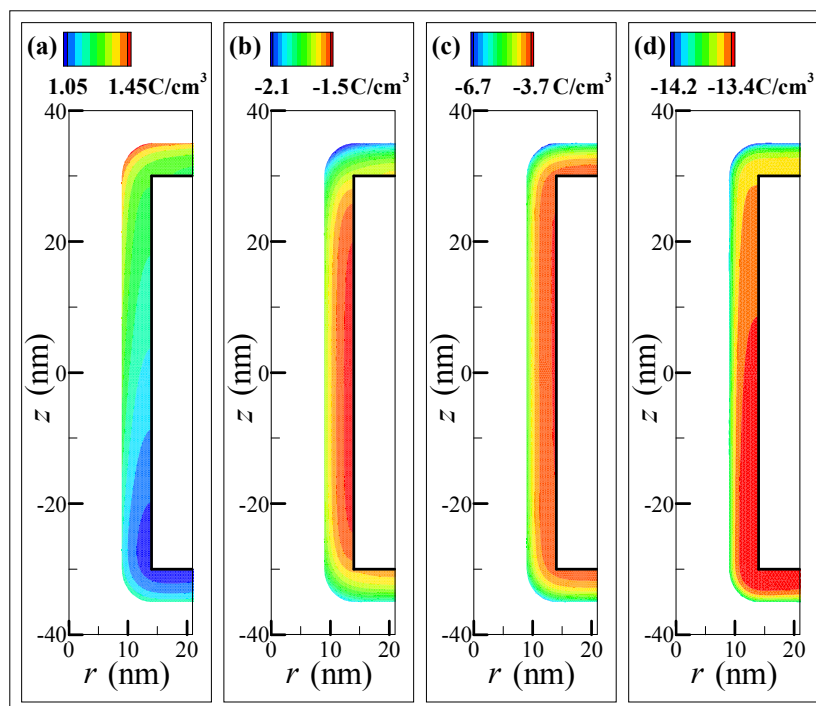
**Fig. 3.** Schematic illustrations of the significant ICP phenomena in a pH-tunable PE layer-modified nanopore if the solution pH is apparently higher, (a), and lower, (b), than the IEP of PE layer. Note that in the former case, the ICP effect is particularly significant under the condition of sufficiently large  $\sigma_m$ , high pH, and low  $C_b$ . The dotted circle in Fig. 3b highlights the enhancement of  $\text{H}^+$  ions near the anode side opening of nanopore.  $\mathbf{J}^-$  and  $\mathbf{J}^+$  denote the ionic fluxes from net anions and cations, respectively. The ionic fluxes inside the nanopore, and at the cathode and anode sides of reservoirs are subscripted as  $np$ ,  $ca$ , and  $an$ , respectively.



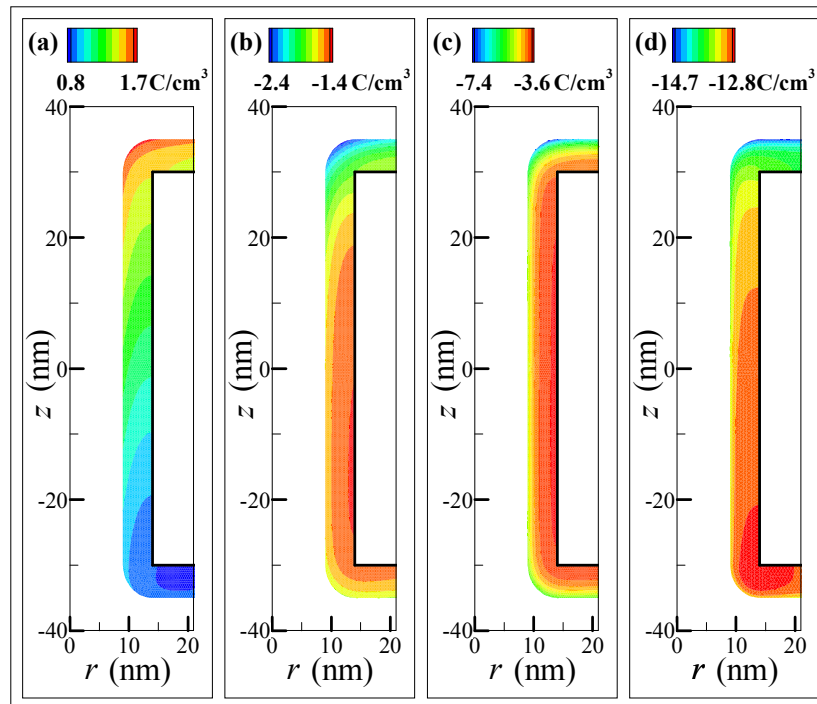
**Fig. 4.** Axial variations of the cross-section-averaged concentrations of  $\text{H}^+$  ions,  $c_{a1}$ , (a), (c), and (e), and net cations,  $c_{a1} + c_{a2}$  (solid lines), and net anions,  $c_{a3} + c_{a4}$  (dashed lines), (b), (d), and (f), for two levels of  $V_0$  at  $\sigma_m = 0.1$  chains/nm<sup>2</sup> and  $C_b = 1$  mM. (a)-(b): pH = 2.2; (c)-(d): pH = 5; (e)-(f): pH = 9. A scale of  $10^2$  and  $10^6$  are, respectively, applied to all curves in Fig. 4c and e for clear visualization. The dotted lines in Fig. 4a, c, and e are the results of the bulk concentration of  $\text{H}^+$  ions,  $c_{a1} = 10^{(3-\text{pH})}$ . The blue region highlights the interior of nanopore.



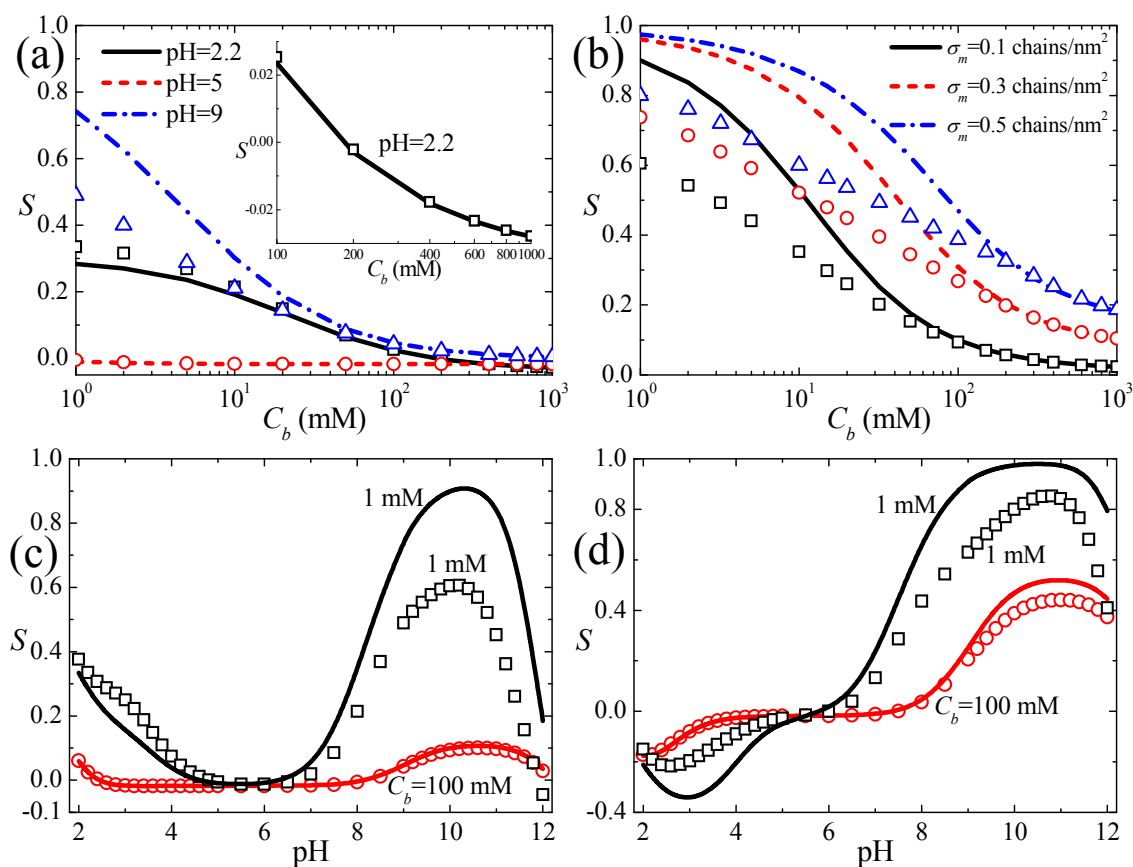
**Fig. 5.** Axial variations of the cross-section-averaged concentrations of  $\text{H}^+$  ions,  $c_{a1}$ , (a), (c), and (e), and net cations,  $c_{a1} + c_{a2}$  (solid lines), and net anions,  $c_{a3} + c_{a4}$  (dashed lines), (b), (d), and (f), for two levels of  $V_0$  at  $\text{pH} = 10$ . (a)-(b):  $\sigma_m = 0.1$  chains/ $\text{nm}^2$  and  $C_b = 1$  mM; (c)-(d):  $\sigma_m = 0.5$  chains/ $\text{nm}^2$  and  $C_b = 1$  mM; (e)-(f):  $\sigma_m = 0.5$  chains/ $\text{nm}^2$  and  $C_b = 100$  mM. The dotted lines in Fig. 4a, c, and e are the results of  $c_{a1} = 10^{-7}$  mM. A scale of  $10^7$  is applied to all curves in Fig. 5a, c, and e for clear visualization. The blue region highlights the interior of nanopore.



**Fig. 6.** Spatial variations of the volume charge density,  $\rho_m$  ( $\text{C}/\text{cm}^3$ ), in the PE layer of biomimetic nanopores for various combinations of pH,  $C_b$ , and  $\sigma_m$  at  $V_0 = 0.2$  V. (a): pH = 2.2,  $C_b = 1$  mM, and  $\sigma_m = 0.1$  chains/ $\text{nm}^2$ ; (b): pH = 10,  $C_b = 1$  mM, and  $\sigma_m = 0.1$  chains/ $\text{nm}^2$ ; (c): pH = 10,  $C_b = 1$  mM, and  $\sigma_m = 0.5$  chains/ $\text{nm}^2$ ; (d): pH = 10,  $C_b = 100$  mM, and  $\sigma_m = 0.5$  chains/ $\text{nm}^2$ .

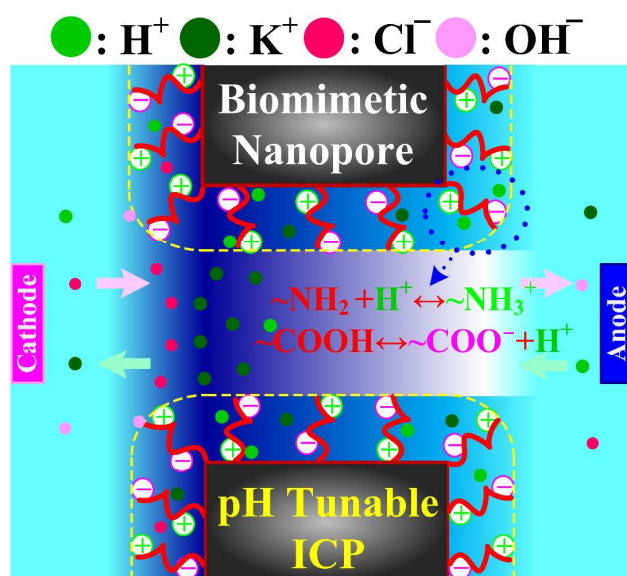


**Fig. 7.** Spatial variations of the volume charge density,  $\rho_m$  ( $\text{C}/\text{cm}^3$ ), in the PE layer of biomimetic nanopores for various combinations of pH,  $C_b$ , and  $\sigma_m$  at  $V_0 = 1 \text{ V}$ . (a): pH = 2.2,  $C_b = 1 \text{ mM}$ , and  $\sigma_m = 0.1 \text{ chains}/\text{nm}^2$ ; (b): pH = 10,  $C_b = 1 \text{ mM}$ , and  $\sigma_m = 0.1 \text{ chains}/\text{nm}^2$ ; (c): pH = 10,  $C_b = 1 \text{ mM}$ , and  $\sigma_m = 0.5 \text{ chains}/\text{nm}^2$ ; (d): pH = 10,  $C_b = 100 \text{ mM}$ , and  $\sigma_m = 0.5 \text{ chains}/\text{nm}^2$ .



**Fig. 8.** Ion selectivity ( $S$ ) of the nanopore as a function of the background salt concentration  $C_b$  for various pHs at  $\sigma_m = 0.1$  chains/nm<sup>2</sup>, (a), and for various  $\sigma_m$  at pH=10, (b), and as a function of pH for two levels of  $C_b$  at  $\sigma_m = 0.1$  chains/nm<sup>2</sup>, (c), and  $0.5$  chains/nm<sup>2</sup>, (d). Lines and symbols denote the results for  $V_0 = 0.2$  V and  $1$  V, respectively. “□”, “○”, and “△” in (a) denote the results for pH = 2.2, 5, and 9, respectively, and in (b) denote the results for  $\sigma_m = 0.1, 0.3,$  and  $0.5$  chains/nm<sup>2</sup>, respectively. Inset in (a) highlights the result of ion selectivity at pH = 2.2 for  $C_b$  in the range of 100-1000 mM.

## TOC Graphic



The ion transport and selectivity in biomimetic nanopores with pH tunable, zwitterionic, polyelectrolyte brushes are investigated theoretically.